JOURNAL OF MECHANICAL ENGINEERING AND SCIENCES
ISSN: 2289-4659 e-ISSN: 2231-8380
VOLUME 19, ISSUE 3, 2025, 10698 - 10712
DOI: https://doi.org/10.15282/jmes.19.3.2025.1.0839

RESEARCH ARTICLE

Mesh independence study for an onshore Oscillating Water Columns using Richardson's extrapolation: Numerical and analytical analysis

J. D. Parra Quintero*

Grupo de Investigación Navarra Ingenierías, Facultad de Ingenierías, Arquitectura y Urbanismo, Fundación Universitaria Navarra, 410001, Neiva, Huila, Colombia
Phone: +57-608-8722049, Fax.: +57-608-8722049

ABSTRACT - Wave energy converters can be a promising option for wave energy, which is among them, aims to be a crucial device for new studies and essential for energy transformation due to its geographical versatility and adaptation to different wave conditions, still being the subject of research and development in the field of renewable energy. The spatial study to evaluate the behavior of Oscillating Water Columns (OWCs) has been a significant challenge in the simulated analysis of these devices due to their high computational cost. OWC is a device that harnesses the oscillatory motion of seawater inside a partially submerged chamber. This movement compresses and decompresses the air column above, driving a turbine connected to a generator and converting wave energy into usable electricity. This study aimed to evaluate the spatial and temporal mesh independence of an onshore OWC using Computational Fluid Dynamics (CFD) and Richardson's Extrapolation (RE). The CFD analysis was performed using ANSYS Fluent software, and a RE study was conducted to enhance the accuracy of the results by extrapolating solutions for different efficiency values obtained from varying domain discretization levels. Indeed, 10 treatments were conducted to investigate the spatial (M_0, M_1, M_2, M_3, and M_4) and temporal (M_2T_1, M_2T_2, M_2T_{1to2}, M_2T_3, and M_2T_4) mesh independence. The results demonstrate, in addition to the inclusion of the analytical second-order Stokes equation, that RE was instrumental in testing the incoming wave front, observing the behavior of the OWC, and reducing its computational cost. M_2 and $M_2T_1to_2$ were the treatments chosen for the spatial and temporal independence analysis, respectively. The extrapolated values correspond to approximately 28.0227% (M_2) and 33.5412% (M2T1 to 2). These findings support the use of RE as a reliable tool for mesh validation in CFD simulations, optimizing computational efficiency while ensuring robust results.

ARTICLE HISTORY
Received : 26th Dec. 2024
Revised : 04th July 2025
Accepted : 17th Sept. 2025
Published : 30th Sept. 2025

KEYWORDS
Analytical modeling
CFD
Richardson's extrapolation
Independence study
Numerical simulation
OWC

1. INTRODUCTION

Nowadays, traditional energy consumption through fossil fuels worldwide has reached a devastating level for the environment, with climate variability, ecosystem loss, and air pollution becoming increasingly concerning. Humanity has used this traditional energy resource to meet the productive processes and activities of modern society (transportation, industry, housing, steam, and electricity generation) [1–3]. Some years ago, the United Nations (UN) established a list of human development goals, whose primary objective is to create a world more rooted in social justice and total equity [4]. Among them, the Sustainable Development Goals stand out, which were adopted in 2015 to address the 2030 Agenda for Sustainable Development. This initiative aims to intensify global efforts to eliminate poverty in all its forms, reduce social disparities, and mitigate climate variability, thereby ensuring sustainability for future generations [5, 6]. The growing demand for energy at the global level, together with the well-founded hopes to address environmental challenges, the commitments and policies of countries around the world to ensure sustainable development for new generations, has managed to focus attention because Non-Conventional Energy Sources (NCES) play a crucial role in the preservation of the environment, energy security and sustainability, its demand has led to the development of innovative technologies, where wave energy can dazzle as a promising option to diversify and decentralize the energy matrix.

Within marine development, wave energy collectors (WECs) have been fundamental for energy utilization for years. These devices enable the capture of wavefront energy through energy systems designed for energy transformation. Among these, the oscillating water column (OWC) stands out as one of the first WECs to be developed and implemented at sea [7]. The OWC, within its pneumatic chamber, utilizes the kinetic energy of the air induced by the incident waves to produce electricity through a self-rectifying turbine [8]. Prominent researchers have studied the OWC. Jasron et al. [9], Falcão [10], Shalby et al. [11, 12], Portillo and Falcão et al. [13–15] and J. Marques Silva et al. [16, 17] have studied the device using analytical models and numerical simulations as well as small-scale or experimental laboratory constructions. Numerical and analytical analysis have become a fundamental link in the study of the OWC. Analytical methods begin with theoretical equations and progress toward exact solutions [18]. Cochran et al. presented the first concept of analytical

***CORRESPONDING AUTHOR | J. D. Parra Quintero** | ✉ jd.parra@uninavarra.edu.co

OWC in 1974 [19]. On the other side, numerical models; allow the simulation of wave interactions with the OWC by means of computational tools [20], in that sense, the Volume of Fluid (VoF) method and the Reynolds Averaged Navier Stokes Equations (RANS) are used for two-dimensional and three-dimensional studies of the device, where the simulation and evolution of the free surface has been of great difficulty [21]. Satrio et al. [22] have employed RANS in Computational Fluid Dynamics (CFD) simulations of a device used to harness the tidal stream.

The combination of both concepts allows not only to validate the results obtained by both methods, but also to address significant CFD phenomena. However, the quality and reliability of the results have often been a problem for researchers, since guaranteeing the safety and reliability of the values obtained for the response variable is not as simple as it might seem at first glance. For this, it is necessary to conduct more in-depth studies on the independence of the mesh domain to be used, ensuring that the response variable does not exhibit sensitivity due to the number of mesh elements or the simulation time step during the calculation method iterations. Few studies [23–27] have devoted their attention to the independence analysis on the response variable of an OWC (efficiency, velocity, pressure, wave height), and the knowledge gap becomes even wider without the use of Richardson Extrapolation (RE) as a reliability method for domain discretization. RE is a numerical method, and one can apply a known order of accuracy, variable step size and estimate a discretization error where it is accurate only in the asymptotic range; when the response variable tends to stabilize its values asymptotically independent of the increase of the mesh refinement [28], in that sense, it allows analyzing the network convergence [29]. It is currently used to increase the order of accuracy of a numerical solution [30], i.e., to improve the order of a formula that approximates a given value [31]. It could even evolve through reduced Richardson extrapolation (RRE), as studied by [32]. It improves the order of a formula that tends to approximate a given value [31]. It could even be evolved by the Reduced Richardson Extrapolation (RRE), as studied by [32], or by the Weighted Richardson Extrapolation (WRE), as studied by [31]. However, the scopes of RRE and WRE have not been considered in this research. Ensuring the quality of the results obtained from the domain discretization, through spatial and temporal independence, is fundamental for the development of the present work.

According to the existing literature, studies about an onshore OWC have focused their research interest on numerical and analytical models. In fact, first order (Airy's theory) [33, 34] and second order Stokes equations [35–37], as well as potential flow theory [38, 39]and linearized water wave theory [40]. Zhou et al. [41] mathematically studied onshore OWCs embedded in a breakwater, which is a structure used to protect coastal areas from erosion. Indeed, they employed parametric studies to investigate the device's performance. The authors found that incorporating multifunctionality through the consideration of more than one resonant chamber for the OWC could significantly enhance wave energy harvesting. Samak et al. [42] studied the contribution of an L-shape attached to the front wall of the resonant chamber. For this, they initially checked the incident wave profile using the analytical equation of the second-order Stokes theory and, through ANSYS-Fluent, the most widely used CFD code in the study of OWCs [43]. They studied three regions over which they divided the computational domain (region 1, water surface area: Δx= 0.025 m, Δz= 2H/20, region 2: Δx = 0.025 m, Δz = 0.025 m, region 3: Δx = 0.025 m, Δz = (chamber inner air region)/30), where H is the wave height. The authors found an excellent correlation between the two methods. Then, they found that the particular shape of the front wall is significant for average efficiency and could be further explored in future studies. [44], To study the influence of various wavelengths and shapes of the resonance chamber bottom, they employed a mesh independence study, which yielded excellent results for variables such as pressure, P, and inner wave elevation, η, measured inside the resonance chamber of the device. Indeed, the discretization of the domain was carried out as follows: i) Δx= Δz = 0.0325 m, ii) Δx= Δz = 0.025 m, and iii) Δx= Δz = 0.0175 m. It was concluded that the second assumption (Δx= Δz = 0.025 m) has adequate resolution to be used in the numerical calculations since it practically coincides with the fifth-order Stokes wave employed. The authors did not study time independence.

Wang & Zhang [35] utilized OpenFOAM software to investigate an offshore OWC, verifying the numerical simulation results against those obtained from Airy's theory. For this reason, the researchers also did not conduct a temporal and spatial mesh independence analysis. Palmer et al. [45] demonstrated that a dual chamber design could improve the performance of an onshore OWC, in that sense, the authors employed CFD to study the device and implemented a spatial independence analysis using three meshes defined as coarse (element size= 0.003m, Δx_{max}= λ/70), intermediate (element size= 0.002m, Δx_{max} = λ/80) and fine (element size= 0.001m, Δx_{max}= λ/90), where the water surface and the interior of the chamber were the most refined regions. The channel length (L_A) was four times the wavelength (λ), equal to the channel length employed in this investigation. The intermediate mesh was used by the authors, given its resemblance to the fine and coarse meshes, as well as its desirable low computational cost. Evidently, one of the significant challenges of CFD is oriented with the accuracy of the numerical results, although, several researches have investigated about the hydrodynamic behavior of an OWC and the discretization of its domain in space and time for the numerical simulation of the device by means of software such as ANSYS-Fluent [36, 37, 46, 47], and ANSYS-CFX [48, 49], OpenFOAM [50–52] or DualSPHysics [53, 54] However, there are still knowledge gaps regarding the study of independence and its analysis using the RE method.

This research aims to numerically and analytically analyze the spatial and temporal mesh independence of an onshore OWC model utilizing the RE method. Under this scenario, the hydrodynamic performance of the prototype is analyzed. During the simulations, the RANS model was coupled to the standard k-ε model and the Pressure-Implicit with Splitting Operators (PISO) method. The methodology and numerical results were validated by analytical equations (to check the incoming wave front) as reported in [42].

2. MATERIAL AND METHODS

2.1 Oscillating Water Column

An OWC is a type of WEC that harnesses the energy of both regular and irregular incident waves by means of a resonance chamber, where a column of water oscillates periodically in a consistent manner, forcing the displacement of water and, therefore, of air in an upward and downward direction. As a result, the pneumatic fluid drives a bidirectional turbine, i.e., one that rotates in the same direction regardless of the flow direction, to feed an electric generator [55]. Figure 1 schematically depicts the device. Figure 1(a) and 1(b) correspond to an offshore and onshore OWC, respectively. In this research, an onshore OWC was employed. Its scope only extends up to the simulation stage, without considering the turbine and its restrictive and compressive effects, which it could have on it, so these have not been taken into account. Indeed, a very small diameter has been considered to generate the damping that a turbine would produce on the pneumatic chamber of the OWC, as it has been considered by [56–59].

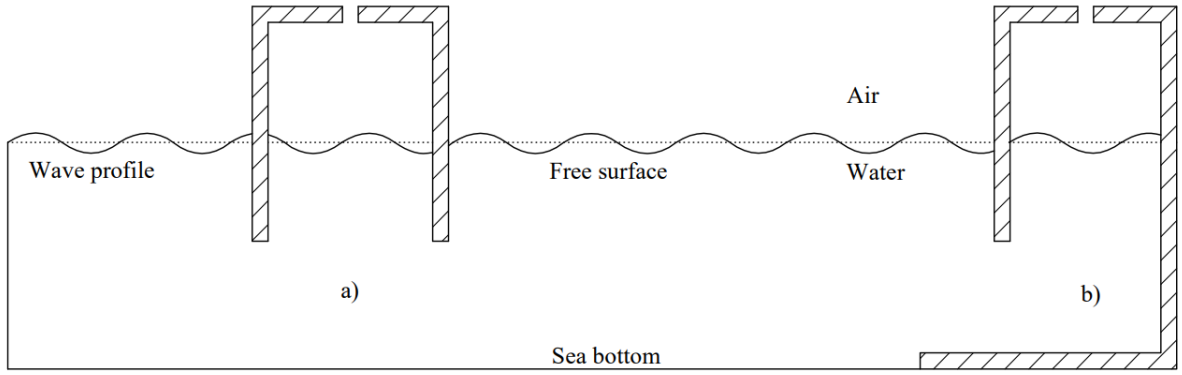

Figure 1. Representation of an OWC: (a) offshore and (b) onshore

2.2 Wave Characteristic and Computational Dominance

Figure 2 corresponds to the schematic representation of the computational domain used in this research. The parameters related to wave characteristics are the incoming wave height, H, the water depth, h, and the wavelength, λ. In this work, the values H = 20, h = 225, and λ = 1470 mm were used to generate the incoming wave front using ANSYS Fluent software for open-channel velocity input. According to the Le Méhauté theory and the wave conditions studied, the appropriate wave theory can be verified. In that sense, and according to what is understood in studies about the subject, such as those of [60–62] and [63], a value of $h/(gT^2)$= 0.01814 for the abscissa and $H/(gT^2)$= 0.00161 for the ordinate was obtained. Therefore, the Stokes second-order theory model has been selected for this research. T is the incident wave period and can be calculated by Eq. (1) [64]. Equation (2) corresponds to the water level elevation η(x,t), for a location x and time t [42], where the wave number, k, is calculated as 2π/ λ and the angular frequency, ω as 2π/T [65], for the wave characteristics described in the previous paragraph, a period of 1.1241s was obtained.

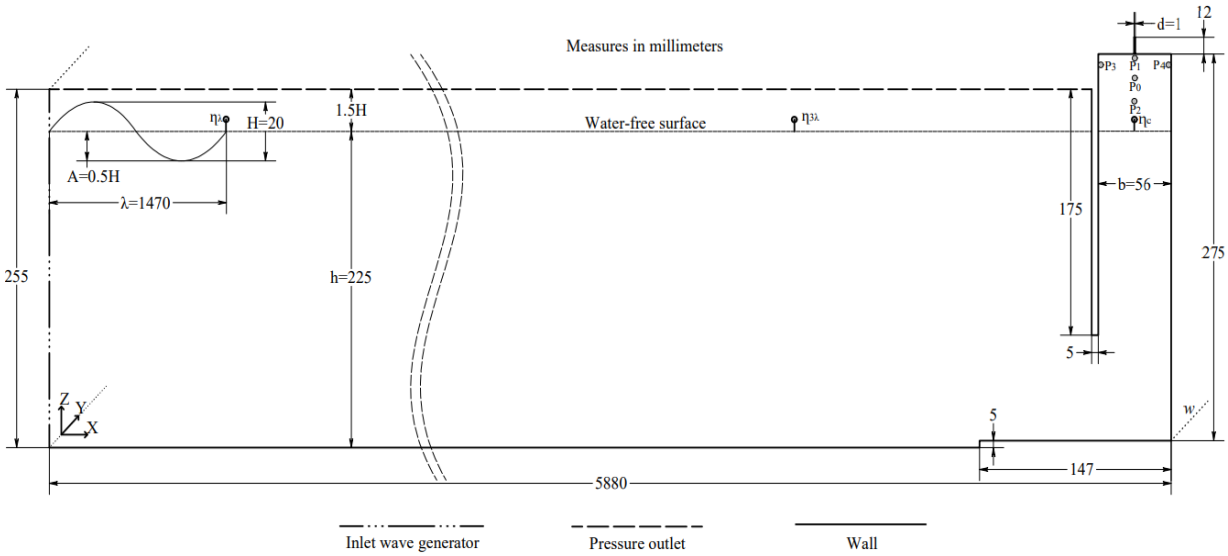

Figure 2. Dimensions of the OWC

$$T = \sqrt{\frac{2\pi\lambda}{g\tanh(2\pi h/\lambda)}} \tag{1}$$

$$\eta(x,t) = \frac{H}{2}\cos(kx-\omega t) + \frac{H^2 k}{16}\frac{\cosh(kh)}{\sinh^3(kh)}[2+\cosh(2kh)]\cos 2(kx-\omega t) \tag{2}$$

2.3 Hydrodynamic Performance

The hydrodynamic performance, ε, of the OWC has been a variable of great interest to some researchers [38, 47, 52, 66], and can be calculated as seen in Eq. (3) [35]. The incident power, $P_{inc,}$ can be calculated using Eq. (4), as described by [42] and associated with the second-order Stokes theory. In this situation, the incident power value obtained by replacing the described values corresponds to 0.5046 (W/m).

$$\varepsilon = \frac{P_{out}}{P_{inc} w} \tag{3}$$

$$P_{inc} = \frac{1}{16}\rho g H^2 \frac{L}{T}\left[1+\frac{2kh}{\sinh(2kh)}\right]\left(1+\frac{9H^2}{64k^4h^6}\right) \text{ (W/m)} \tag{4}$$

The pneumatic power available at the output, $P_{out,}$ can be calculated using Eq. (5) [38, 42, 63], where T_a and T_b correspond to the initial and final interval over which the power available at the OWC output is determined for the efficiency calculation. In this work, efficiency is calculated in the range covering [T_a, T_b] for the region where the P_{out} curve stabilizes ($t > T_a$), as presented in the results section later.

$$P_{out} = \frac{1}{T_b - T_a}\int_{T_a}^{T_b} \Delta P * Q(t)\, dt \ (W) \tag{5}$$

The ΔP and Q(t) correspond to the pressure change and the air flow rate inside the resonant chamber, respectively. It is necessary to emphasize that ΔP does not refer to the subtraction between the values of two pressure monitors (otherwise ΔP would be almost zero), but, rather, it corresponds to the change in the pressure curve product of the internal oscillations generated inside the OWC, this can be corroborated in investigations that have used only one pressure monitor [42, 67] and two [35, 68–70], where even for the second case they were averaged. As the computational domain studied is in two dimensions (2D), some authors have attributed that Q(t) can be calculated as an area times a velocity which has been named $S_{chamber} * V_{FS}$ [35, 42, 69], where $S_{chamber}$ is the area of the internal fluid exposed in the chamber and is calculated as b*w, where b is the length of OWC (see Figure 2), and the parameter w, corresponds to the extruded width in the Y-axis direction. However, since in a 2D domain, the extrusion in that direction is zero, w should be taken as 1, as assumed in the investigations of authors such as [35, 42, 68–70]. V_{FS} corresponds to the velocity of the internal water surface in the resonant chamber of the OWC and can be calculated using Eq. (6), where Δt represents the step size used in the simulation. Finally, a new method for calculating P_{out} in a 2D domain is presented in Eq. (7).

On the other hand, in this research, the discretization of the domain has been carried out by dividing it into mesh regions to minimize computational costs and also to be able to refine the areas where there are large gradients, such as the surface area of the water and the inner area of the resonant chamber. In this sense, the domain was divided into ten regions (see Figure 3). Table 1 represents the ranges and values over which the regions were comprised for the five meshes studied (M_4, M_3, M_2, M_1, and M_0).

$$V_{FS} = \dot{\eta}_c = \frac{d[\eta_c(x,t)]}{dt} = \frac{\Delta\eta_c}{\Delta t} = \frac{\eta_{c_{i+1}} - \eta_{c_i}}{t_{i_{+1}} - t_i} \tag{6}$$

$$P_{out} = \frac{bw}{T_b - T_a}\int_{T_a}^{T_b} \Delta P V_{FS}\, dt \tag{7}$$

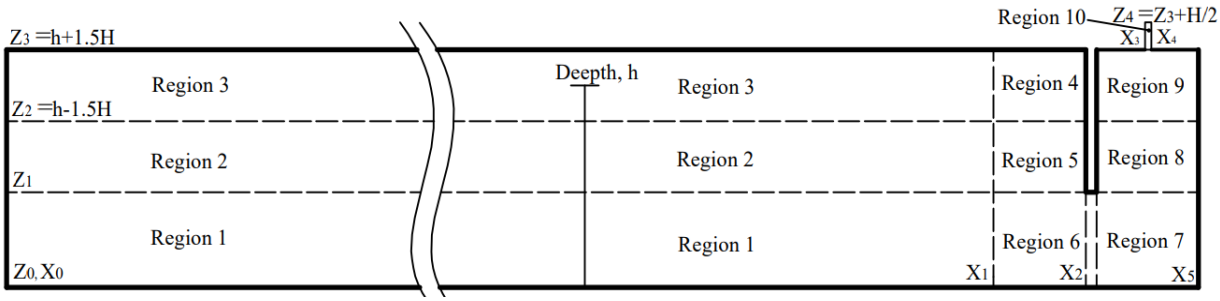

Figure 3. Discretization of the domain through regions

Table 1. Ranges and considerations for the discretization of the mesh in each of the regions included in the studied domain

		Mesh considerations					Mesh values (meters)				
		M_4	M_3	M_2	M_1	M_0	M_4	M_3	M_2	M_1	M_0
Region 1: $X_0 \leq X \leq X_1$, $Z_0 \leq Z \leq Z_1$	dx_1	λ/50	λ/100	λ/200	λ/300	λ/500	0.0294	0.0147	0.0074	0.0049	0.0029
	dz_1	3H/30	3H/40	3H/45	3H/50	3H/100	0.0020	0.0015	0.0013	0.0012	0.0006
Region 2: $X_0 \leq X \leq X_1$, $Z_1 \leq Z \leq Z_2$	dx_3	λ/50	λ/100	λ/200	λ/300	λ/500	0.0294	0.0147	0.0074	0.0049	0.0029
	dz_3	3H/25	3H/35	3H/40	3H/45	3H/80	0.0024	0.0017	0.0015	0.0013	0.0008
Region 3: $X_0 \leq X \leq X_1$, $Z_2 \leq Z \leq Z_3$	dx_2	λ/50	λ/100	λ/200	λ/300	λ/500	0.0294	0.0147	0.0074	0.0049	0.0029
	dz_2	3H/20	3H/30	3H/35	3H/40	3H/60	0.0030	0.0020	0.0017	0.0015	0.0010
Region 4: $X_1 \leq X \leq X_2$, $Z_2 \leq Z \leq Z_3$	dx_5	λ/200	λ/400	λ/500	λ/600	λ/800	0.0074	0.0037	0.0029	0.0025	0.0018
	dz_5	3H/20	3H/30	3H/35	3H/40	3H/60	0.0030	0.0020	0.0017	0.0015	0.0010
Region 5: $X_1 \leq X \leq X_2$, $Z_1 \leq Z \leq Z_2$	dx_4	λ/200	λ/400	λ/500	λ/600	λ/800	0.0074	0.0037	0.0029	0.0025	0.0018
	dz_4	3H/25	3H/35	3H/40	3H/45	3H/80	0.0024	0.0017	0.0015	0.0013	0.0008
Region 6: $X_1 \leq X \leq X_2$, $Z_0 \leq Z \leq Z_1$	dx_6	λ/200	λ/400	λ/500	λ/600	λ/800	0.0074	0.0037	0.0029	0.0025	0.0018
	dz_6	3H/30	3H/40	3H/45	3H/50	3H/100	0.0020	0.0015	0.0013	0.0012	0.0006
Region 7: $X_2 \leq X \leq X_5$, $Z_0 \leq Z \leq Z_1$	dx_7	λ/2450	λ/2940	λ/3675	λ/5880	λ/5880	0.0006	0.0005	0.0004	0.0003	0.0003
	dz_7	3H/30	3H/40	3H/45	3H/50	3H/100	0.0020	0.0015	0.0013	0.0012	0.0006
Region 8: $X_2 \leq X \leq X_5$, $Z_1 \leq Z \leq Z_2$	dx_8	λ/2450	λ/2940	λ/3675	λ/5880	λ/5880	0.0006	0.0005	0.0004	0.0003	0.0003
	dz_8	3H/35	3H/45	3H/50	3H/55	3H/95	0.0017	0.0013	0.0012	0.0011	0.0006
Region 9: $X_2 \leq X \leq X_5$, $Z_2 \leq Z \leq Z_3$	dx_9	λ/2450	λ/2940	λ/3675	λ/5880	λ/5880	0.0006	0.0005	0.0004	0.0003	0.0003
	dz_9	3H/40	3H/50	3H/55	3H/60	3H/135	0.0015	0.0012	0.0011	0.0010	0.0004
Region 10: $X_3 \leq X \leq X_4$, $Z_3 \leq Z \leq Z_4$	dx_{10}	d/2	d/2	d/2	d/4	d/4	0.0005	0.0005	0.0004	0.0003	0.0003
	dz_{10}	3H/60	3H/80	3H/120	3H/180	3H/210	0.0010	0.0008	0.0005	0.0003	0.0003

2.4 Validation

To validate the methodology used in this research, the Type B model studied by [42] was replicated in this research. For this purpose, the open-channel velocity inflow contour was initially used to generate the incoming wave front, using the parameters H = 0.12 m, λ = 7.3 m, and h = 0.92 m, as specified by the authors as mentioned above. The air zone in the channel and the outflow of this fluid from the chamber were considered as a pressure outflow (0 Pa). The remaining contours were regarded as a wall. ANSYS Fluent software was used to solve the equations of motion for fluid flow based on the RANS model, which was coupled with the PISO method and the k-ε standard turbulence model. This model is used by the noted authors and in studies such as [71] and [47].

Regarding the discretization of the domain, the implicit first-order approach was employed. A time step, Δt of 0.01 s was employed, where the convergence criterion for the residuals per iteration was 10^{-3}. For the P_{inc} calculation, Eq. (3) was employed. As for the hydrodynamic parameters corresponding to P_{out}, the CFD- Post component system of ANSYS-Fluent was necessary to employ to calculate ΔP and $\eta_{chamber}$, which, corresponds to the log of the rise and fall of the water level at the shallow center inside the resonant chamber, with this parameter V_{FS} was determined by Eq. (6). Figure 4 represents the numerical values obtained from the simulation for the validated model. Figure 4(a-b) illustrates the application of the analytical and numerical model to the model analysis. Authors such as [35] have employed this type of analytical and numerical comparison within their research methodology. Figure 4(c-e) corresponds to the results of V_{FS}, ΔP, and P_{out}, respectively. It is observed that from 12.96 s, these three curves stabilized.

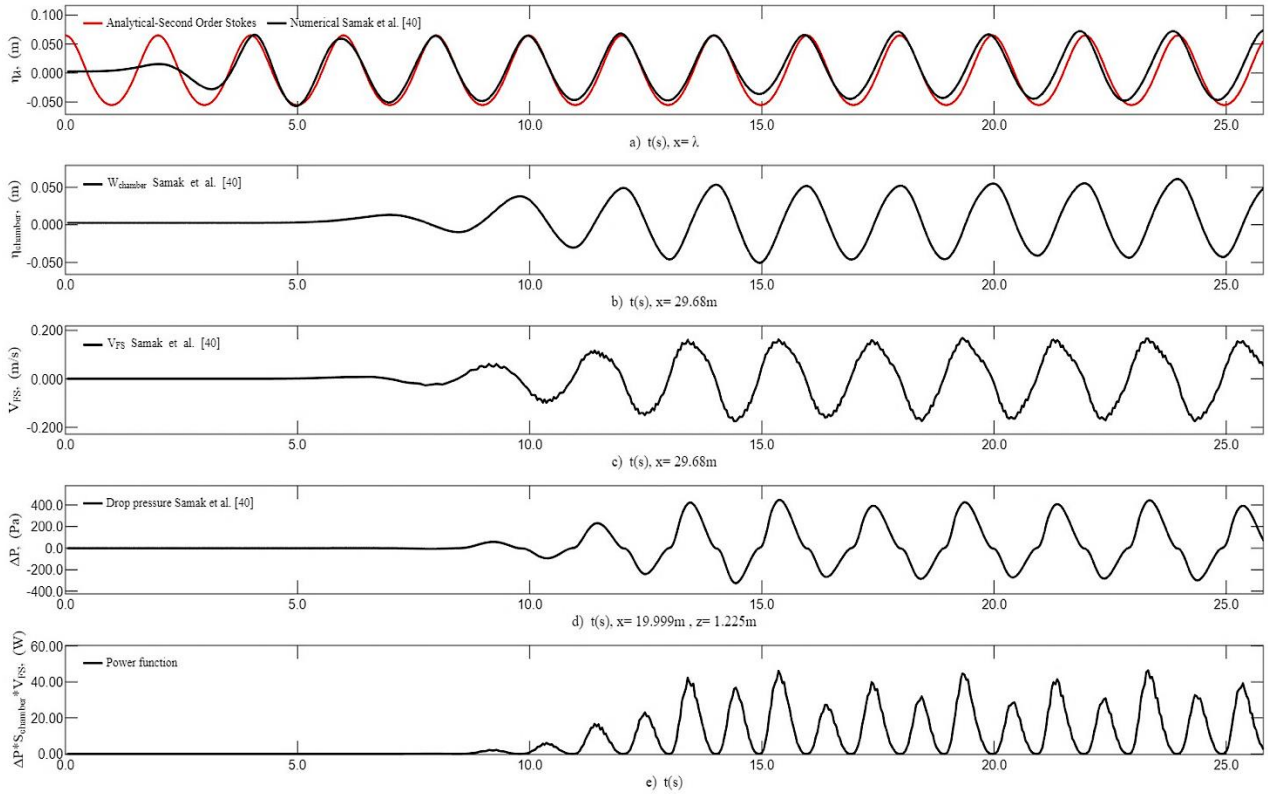

Figure 4. Numerical parameters obtained from the research published by [42], figure adapted

2.5 Treatments

In this research, 10 treatments were used to study mesh independence. Regarding spatial independence, the treatments M_4, M_3, M_2, M_1, and M_0 were used for analyzing the mesh structure in the computational space. Table 2 presents the spatial network parameters, including the number of elements, nodes, average aspect ratio, average asymmetry, and simulation time, for each treatment, as performed on an ASUS computer with an AMD Ryzen 5 3500U processor. Figure 5 represents the mesh of the spatially studied treatments, where Figure 5(a) shows the computational domain. In the final zone towards X_{max}, the red and blue boxes correspond, as can be seen, to the amplified capture of the mesh on the side where the OWC is and its interior, respectively. Similarly, for the time independence study, five treatments (M_2T_4, M_2T_3, M_2T_2, M_2T_1, and M_2T_{1to2}) were performed, where the step sizes used corresponded to 0.0075, 0.005, 0.0025, 0.00125, and 0.001875s, respectively.

Table 2. Mesh independence study

Mesh Parameters	M_4	M_3	M_2	M_1	M_0
Number of elements	37774	85768	172017	289811	799458
Number of nodes	38325	86626	173345	291668	802448
Average aspect ratio	8.0131	6.7700	4.5232	3.8088	3.8009
Average skewness	5.3621×10^{-5}	5.5942×10^{-7}	2.5182×10^{-5}	3.6269×10^{-7}	2.1581×10^{-6}
Simulation time	8 h 30 min	13h 41 min	34h 8 min	59 h and 5 min	154 h 7 min

2.6 Numerical Simulation

ANSYS has been used to determine ε through a series of CFD studies on the indicated treatments. The RANS equations were employed for the fluid simulation process using this software. Table 3 presents the adjustments carried out through the Fluent package. It is essential to note that previously, the geometry had to be inserted, the contours had to be named, and the meshing process had to be carried out. Up to this point, to determine ε, it is necessary to carry out one final step, which CFD-Post performs to obtain ΔP and V_{FS}, as described in [42].

2.7 Richardson's Extrapolation

The most widely applied technique for studying both spatial and temporal mesh independence is the Grid Convergence Index (GCI) [72], which can be based on the RE method [28, 73]. It is known that if GCI is close to unity, the solution obtained from the technique is considered reliable and remains unchanged as the element size and step size decrease [74].

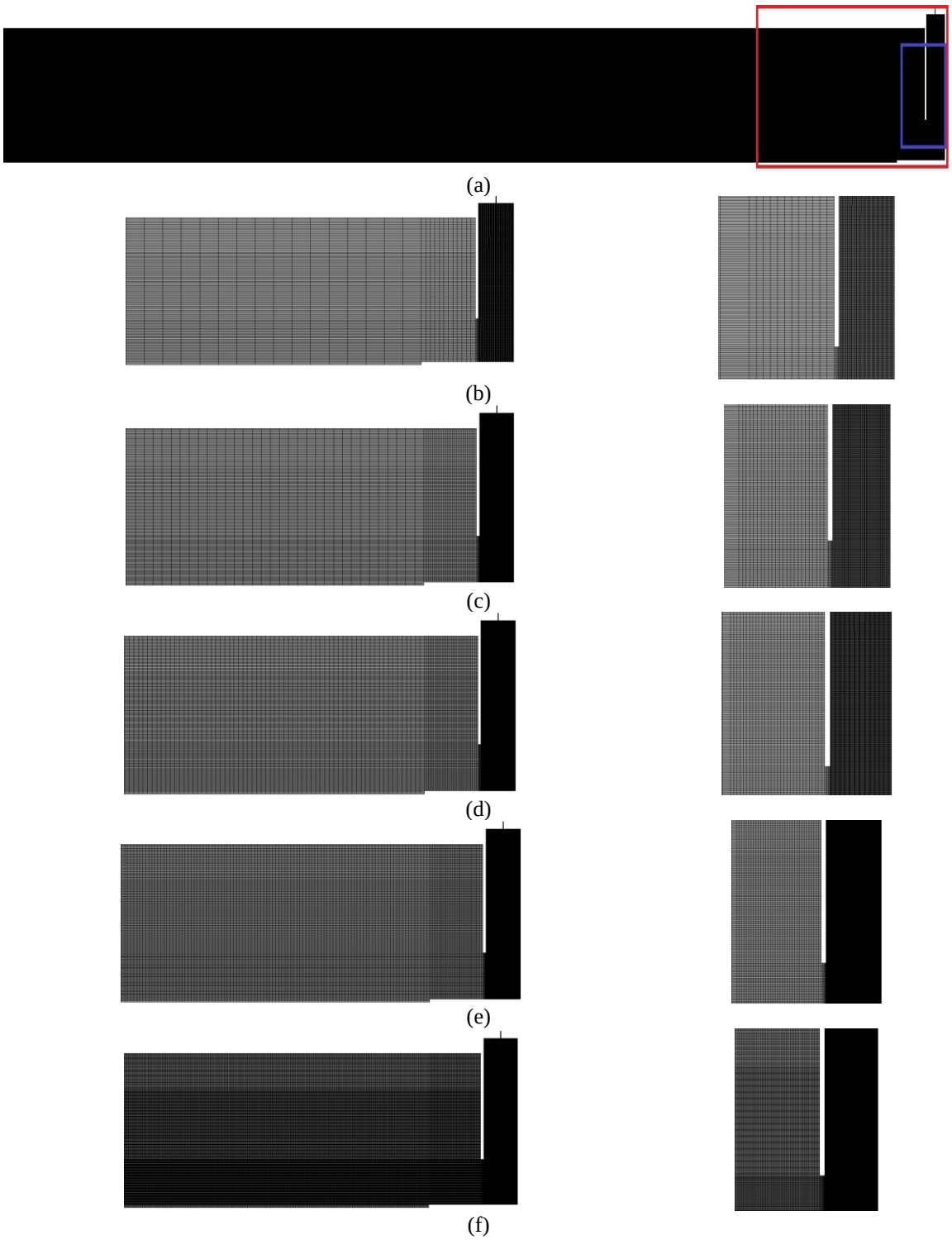

Figure 5. Discretization and mesh refinement for the study of spatial independence: (a) computational domain studied, (b) M_4, (c) M_3, (d) M_2, (e) M_1, and (f) M_0

The inclusion of RE within the investigation allows for the selection of a convenient mesh and step size to minimize computational cost [75]. GCI can be computed by: i) choosing a parameter, f_i, which in this work was associated with ε_i, ii) choosing a value in the refinement constant (r), where it should be guaranteed that $r > 1.1$ [74, 76], before this restriction, r is commonly taken with a value of 2, iii) the simulation of three spatial treatments corresponding to the fine, medium and coarse mesh with ε_1, ε_2 and ε_3, respectively, iv) the calculation of the convergence order, p given by Eq. (8), v) the calculation of $\varepsilon_{h=0}$ using Eq. (9), where h corresponds to the separation between mesh elements, in this case, h tends to zero value, vi) the calculation of GCI_{12} and GCI_{23} using Eqs. (10) and (11), respectively, vii) the calculation of GCI by means of Eq. (12), where Fs is called the safety factor and has a value of 1.25 [74, 75]. The obtained value of GCI should be very close to 1 [74]. Once these six steps are carried out, the solution is determined by the RE method.

Table 3. Model configuration in ANSYS-Fluent

Setup	Considerations	
General	Gravity	-9.81 m/s
	Transient	Active
Models	Multiphase	Volume of Fluid (VoF)
	Viscous	Standard k-e
Materials	Fluid	Air (default)
		Water (default)
Boundary conditions	Velocity inlet (wave profile)	Open Channel Wave BC
		Multiphase (H, h, wave theory)
	Oulet	Pressure outlet (Gauge pressure=0 Pa)
	Wall	Default
Solution	Methods	PISO, PRESTO, default
	Residuals	10^{-3}
	Initialization	Hybrid, patch (create water region)
	Autosave	0.03 s
	Max iterations/Time step	30

2.8 Study of Mesh Independence

To evaluate the mesh independence of the OWC model shown in Figure 2, the process was carried out in two stages, one for spatial and the other for temporal discretization. The first stage involved studying spatial mesh independence, where five different structured meshes (M_0 to M_4) were generated with increasing refinement as a function of λ, with a particular focus on regions with higher gradients, such as the free surface and the air-water interface within the resonance chamber. In this regard, the number of nodes, elements, average aspect ratio, skewness level, and simulation time were recorded to evaluate the computational cost of the simulated device (see Table 2). For the five spatial meshes considered, ε was calculated from the results obtained with CFD-Post (presented in the following section), ΔP, and VFS on the pneumatic chamber, according to Eqs. (3) to (7) outlined in section 2.3, in this regard, three representative meshes (coarse, medium, and fine) were selected to apply RE and GCI, as described in the previous section.

The second stage consisted of studying the independence of the time step size, using mesh M2 (medium mesh) as a basis, and evaluating five different time step values: Δt = 0.0075, 0.005, 0.0025, 0.001875, and 0.00125 s. ε was recalculated for each Δt, and the sensitivity of the results to the different time steps was analyzed, comparing the peaks and the shape of the power curves. Finally, RE and GCI analyses were applied to three representative values of Δt to ensure that the numerical solution was in the asymptotic regime. In the next session, the study's results on the independence of the numerical solution with respect to spatial and temporal discretization parameters will be presented.

3. RESULTS AND DISCUSSION

3.1 Numerical Results

The numerical results obtained from the spatial and temporal independence treatments are presented in Figures 6 and 7, respectively. As can be seen, the simulations were performed up to 15 seconds, a time period during which a steady-state region already exists and a periodic trend of the studied variables (η_λ, $\eta_{3\lambda}$, η_c, ΔP, $V_{FS,}$ and P_{out}) is observed. Figure 6(a-c) corresponds to the incoming wave front monitored from CFD-Post, by means of a wave gauge located at a distance x = λ, x = 3λ, and x = 5.847 m, the latter corresponds to the location of the gauge over the water surface located at the center of the resonant chamber, η_c, as shown in Figure 2. In that sense, η_λ, $\eta_{3\lambda,}$ and η_c correspond to a η(x,t) for each of the gauges as mentioned above. As can be seen, the curve η_c undergoes its first excitation after 5 seconds, the time over which the incident wave takes to reach the interior of the resonance chamber.

The period obtained for η_λ and $\eta_{3\lambda}$ was 1.1481 s, which represents a relative error of 2.09% with respect to the analytical period, T, which was 1.1241 s. ΔP was determined as the change in static pressure over the simulated time. A pressure monitor, $P_{0,}$ was located at X = 5.847 and Z = 0.274 m. One of the doubts that arose through this investigation was regarding the location of the pressure gauge inside the resonant chamber, since, for example, in [42], the pressure gauge was located on the upper right side of the air region inside the chamber (on the back wall and 5 cm from the ceiling). It is for this reason that four additional pressure gauges P (X, Z) for P_1 (5.847, 0.279), P_2 (5.847, 0.262), P_3 (5.820, 0.275), and P_4 (5.875, 0.275), were included and studied in this investigation to contrast the influence of the sensor location versus the curves obtained for ΔP.

$$p = \frac{\ln\left(\frac{\varepsilon_3 - \varepsilon_2}{\varepsilon_2 - \varepsilon_1}\right)}{\ln(r)} \tag{8}$$

$$\varepsilon_{h=0} = \varepsilon_2 + \frac{\varepsilon_1 - \varepsilon_3}{r^p\text{-}1} \tag{9}$$

$$\mathrm{GCI}_{12} = \frac{F_s \left|\frac{\varepsilon_2 - \varepsilon_1}{\varepsilon_1}\right|}{r^p\text{-}1} \tag{10}$$

$$\mathrm{GCI}_{23} = \frac{F_s \left|\frac{\varepsilon_3 - \varepsilon_2}{\varepsilon_2}\right|}{r^p\text{-}1} \tag{11}$$

$$\mathrm{GCI} = \frac{\mathrm{GCI}_{23}}{r^p \mathrm{GCI}_{12}} \tag{12}$$

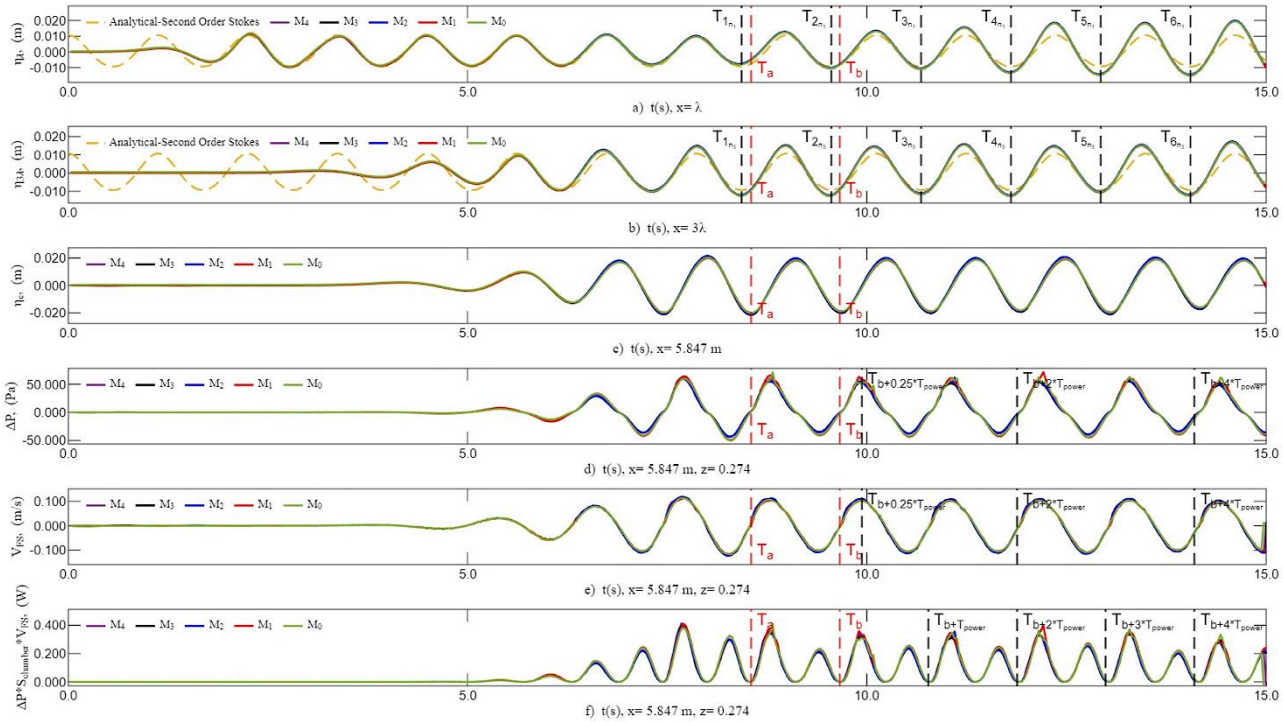

Figure 6. Parameters were studied spatially to calculate the hydrodynamic performance of the OWC

The maximum relative error with respect to ΔP_0 was 5.5563% and corresponded to the ΔP_1 curve. The differences contributing to the lower peaks observed graphically are illustrated in Figure 8. The values used to calculate the error were obtained as the area under the pressure curve in the interval between Ta and Tb. The other relative errors are presented in Table 4. Figure 8 shows the results for ΔP extracted from the analysis. Few changes are observed in terms of morphology and values obtained, indicating that the resonant chamber would behave as a regular pneumatic pressure region. Consequently, ΔP_{prom} was one of the variables selected to solve Eq. (7).

Table 4. ΔP values studied for five pressure points inside the OWC resonant chamber

	Area (Pa*s)	Relative error (%)
P_0	6.9183	-
P_1	6.5339	5.5563
P_2	6.9163	0.0289
P_3	6.8881	0.4365
P_4	6.8858	0.4698

The P_{out} curve obtained from the studied OWC (Figure 6(f) and Figure 7(f)) had a very similar behavior to the extracted pneumatic power, P_E curves reported by [77], allowing to corroborate what was obtained through the validation performed in this research, reported by [42].

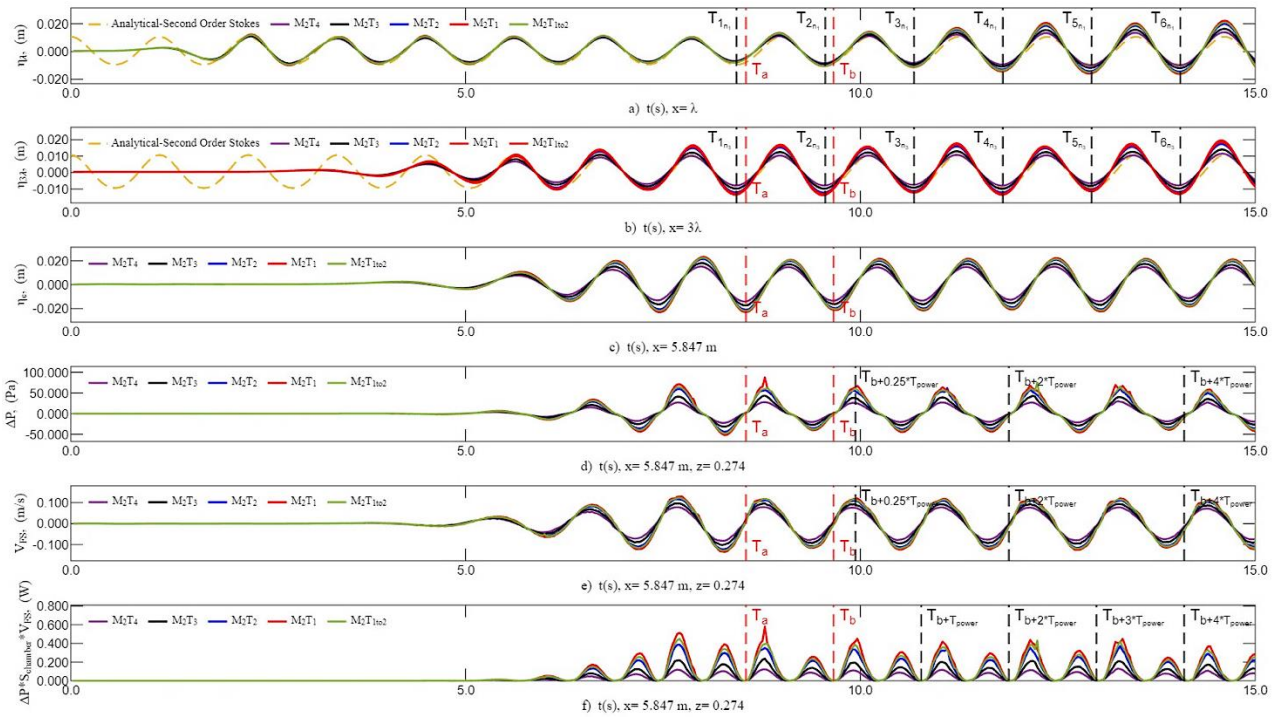

Figure 7. Parameters studied temporarily to calculate the hydrodynamic performance of the OWC analyzed

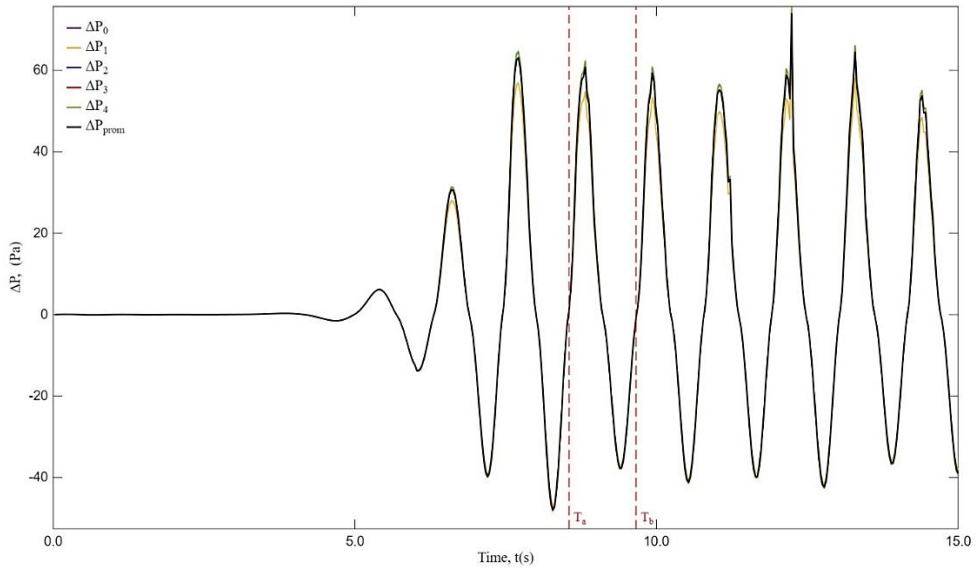

Figure 8. Pressure change, ΔP, at the five points studied, P_0, P_1, P_2, P_3, and P_4

The efficiency values obtained by analyzing the hydrodynamic behavior of the OWC studied in this work are presented in Table 5 and were calculated over the time range between T_a and T_b, corresponding to a period of pneumatic power generation through the OWC. It is necessary to reiterate that ε was determined in the range [T_a, T_b] for all the treatments studied and reported in this research. In Table 5, ε values are tabulated for both spatial and temporal analysis; for the former, out of the five meshes that were studied; three were selected: M_1 (Fine), M_2 (Medium) and M_3 (Coarse), although, M_0 corresponds to a mesh size with a higher number of elements and computational cost than M_4 (799458 vs 37774); its efficiency values (26.6532 vs 26.3246) represented a relative error of 1.2329% with respect to the finest mesh (M_0). M_1 was the mesh where the highest efficiency was obtained, due to the high peaks of the power curve, which makes its area larger. Curiously, ε of M_0 was lower, but it could be due to the disordered power peak in the first movement of the device after T_a and each oscillation period. It is for this reason that, in order to achieve computational balance and conduct the temporal analysis, M_2 has been selected and employed for the second part of the space-time domain analysis. Regarding the temporal independence analysis, Figure 7 presents the results obtained from the numerical analysis of each Δt on the M_2 mesh, specifically M_2T_1, M_2T_2, M_2T_3, M_2T_4, and $M_2T_1to_2$ (an intermediate temporal treatment between M_2T_1 and M_2T_2). As can be seen, the peak values in each oscillation are sensitive to Δt; the lower the step value, the higher the peak tends to be. Similar behaviors have been reported by [45, 47] and [78]. This same methodology focused on analyzing time step refinement using a mesh selected based on spatial independence, as employed by [79]. Of the five temporal

treatments, three were selected under Δt, denoted as high (1), medium (2), and low (3), corresponding to M_2T_1, $M_2T_{1to2,}$ and M_2T_2, respectively.

Table 5. Values obtained from the independence analysis using GCI

	Spatial				Temporal				
Mesh		Efficiency		Relative error (%)	Time step (Δt)		Efficiency		Relative error (%)
--	M_0	--	26.6532	--	0.001250	M_2T_1	ε_1	32.3775	--
Fine (1)	M_1	ε_1	27.4882	3.1328	0.001875	M_2T_{1to2}	ε_2	28.8863	10.7828
Medium (2)	M_2	ε_2	25.8847	2.8833	0.002500	M_2T_2	ε_3	25.8847	20.0534
Coarse (3)	M_3	ε_3	25.6589	3.7305	0.005000	M_2T_3	--	16.0707	50.3646
--	M_4	--	26.3246	1.2329	0.007500	M_2T_4	--	9.7167	69.9893
GCI				1.0619	GCI				1.1209
GC_{12}				-0.0849	GC_{12}				-0.9611
GC_{23}				-0.0127	GC_{23}				-0.9262

Figure 9 represents the results obtained for the independence study and the RE. A Δt of 0.001875 and M_2 have been chosen, as these considerations have small discrepancies with respect to RE, reduce the computational cost, and minimize computational time for future works employing the studied domain. As can be seen, the spatially and temporally extrapolated values correspond to about 28.0227 and 33.5412%, respectively. After implementing RE, the M2T1 to 2 treatment was finally selected. These assumptions not only allow for reducing the computational time but also represent small deviations with respect to the solution obtained by the numerical method.

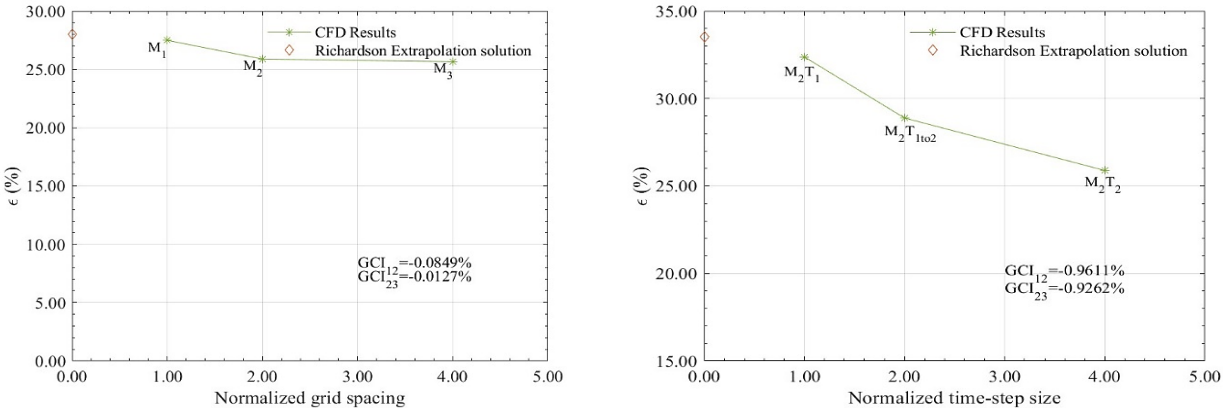

Figure 9. Richardson's extrapolation: (a) mesh independence test and (b) time-step independence test

Once the values obtained from the simulation are extrapolated, the analysis of the OWC behavior is essential, as a consequence, from Figure 6 it can be seen that when the water level inside the resonant chamber is at the lower minimum or upper maximum point, the available pneumatic power is null, however, during that path of ascent of the water column, is where a higher power is generated in the range [T_a, T_a +(T_b-T_a)/2], versus that which would be generated during its descent for the range [T_a+(T_b-T_a)/2, T_b], the same happens in the successive oscillations. V_{FS} and ΔP are in phase, but η_c has a time lag of 0.29 seconds, a time equivalent to almost a quarter of T. Similar results could be deduced from [77].

4. CONCLUSIONS

The mesh independence study, which analyzes an OWC using analytical, numerical, and RE models, is fundamental in providing consistent results. It can be demonstrated that both numerical and analytical analyses show that the simulation responds robustly to changes in mesh resolution, confirming the convergence of the solutions. The use of RE has allowed efficient estimation of model behavior at finer resolutions, providing valuable insights for future work. A GCI of 1.0619 and 1.1209 was obtained using RE for the spatial and temporal independence analysis, respectively. The M2T1 to 2 treatment, with a step size of 0.001875 s, is the most appropriate due to its low computational cost and high reliability in the results. These findings support the validity and accuracy of the model used and highlight the importance of considering network independence in similar studies to ensure reliable results. As future work, studies employing geometric factors and various wave features as sources of investigation can be conducted. The inclusion of multi-camera OWC could be a promising option to study the performance of the OWC presented in this research.

ACKNOWLEDGEMENTS

The Industrial Design and Energy Integration Research Seminar of the university supported this research. The authors have not received any private funding for this study.

CONFLICT OF INTEREST

The authors declare that they have no economic, financial, or personal conflicts of interest that could have compromised the integrity and objectivity of the work presented in this document.

AUTHORS CONTRIBUTION

J. D. Parra Quintero (Writing – review & editing; Methodology; Validation; Supervision, Investigation)

AVAILABILITY OF DATA AND MATERIALS

The data supporting this study's findings are available on request from the corresponding author.

ETHICS STATEMENT

This study did not involve people, animals, or sensitive or confidential personal data. The entire analysis process was carried out in accordance with academic guidelines. The authors have not employed an AI-based tool or AI technology to write this article.

REFERENCES

[1] E. Elnagar, S. Gendebien, E. Georges, U. Berardi, S. Doutreloup, V. Lemort, "Framework to assess climate change impact on heating and cooling energy demands in building stock: A case study of Belgium in 2050 and 2100," *Energy and Buildings*, vol. 298, no. 6, pp. 1–24, 2023.

[2] A. Zhao, Y. Jiao, W. Quan, Y. Chen, "Net zero carbon rural integrated energy system design optimization based on the energy demand in temporal and spatial dimensions," *Renewable Energy*, vol. 222, no. 6, p. 119818, 2023.

[3] C. R. J. Kumar, M. A. Majid, "Renewable energy for sustainable development in India: Current status, future prospects, challenges, employment, and investment opportunities," *Energy, Sustainability and Society*, vol. 10, no. 2, pp. 1–36, 2020.

[4] UNDESA, "Social justice and the United Nations: The divide between human rights and economic and social development," in *Social Justice in an Open World*, United Nations, pp. 51–71, 2006.

[5] UNDP, "The ODS in action," United Nations Development Program, New York, 2015 [Online], Available: https://www.undp.org/africa/waca/sdgs-action

[6] UNDP, "Towards a more equitable, healthy and sustainable future," *Report*, United Nations Development Program, New York, 2022.

[7] A. F. O. Falcão, L. M. C. Gato, "Air turbines," in *Comprehensive Renewable Energy*, pp. 111–149, 2012.

[8] Y. Sang, H. B. Karayaka, Y. Yan, N. Yilmaz, D. Souders, "Ocean (Marine) energy," in *Comprehensive Energy Systems*, pp. 733–769, 2018.

[9] J. U. Jasron, S. Soeparmani, L. Yuliati, D. B. Darmadi, "Comparison of the performance of oscillating water column devices based on arrangements of water columns," *Journal of Mechanical Engineering and Sciences*, vol. 14, no. 3, pp. 7082–7093, 2020.

[10] A. Falcão, "Wave energy utilization: A review of the technologies," *Renewable and Sustainable Energy Reviews*, vol. 14, no. 3, pp. 899–918, 2010.

[11] M. Shalby, A. Elhana, P. Walker, D. G. Dorrell, "CFD modelling of a small–scale fixed multi–chamber OWC device," *Applied Ocean Research*, vol. 88, no. 3, pp. 37–47, 2019.

[12] M. Shalby, A. Elhanafi, P. Walker, D. G. Dorrell, A. Salah, M. R. Gomaa, "Experimental Investigation of the Small-scale Fixed Multi-chamber OWC Device," *Chinese Journal of Mechanical Engineering*, vol. 34, no. 1, 2021.

[13] J. C. C. Portillo, L. M. C. Gato, J. C. C. Henriques, A. F. O. Falcão, "Implications of spring-like air compressibility effects in floating coaxial-duct OWCs: Experimental and numerical investigation," *Renewable Energy*, vol. 212, no. 5, pp. 478–491, 2023.

[14] J. C. C. Portillo, J. C. C. Henriques, L. M. C. Gato, A. F. O. Falcão, "Model tests on a floating coaxial-duct OWC wave energy converter with focus on the spring-like air compressibility effect," *Energy*, vol. 263, no. 9, p. 125549, 2023.

[15] A. F. O. Falcão, J. C. C. Henriques, R. P. F. Gomes, J. C. C. Portillo, "Theoretically based correction to model test results of OWC wave energy converters to account for air compressibility effect," *Renewable Energy*, vol. 198, no. 3, pp. 41–50, 2022.

[16] J. Marques Silva, S. M. Vieira, D. Valério, J. C. C. Henriques, "Model predictive control based on air pressure forecasting of OWC wave power plants," *Energy*, vol. 284, no. 8, p. 129217, 2023.

[17] J. M. Silva, S. M. Vieira, D. Valério, J. C. C. Henriques, "GA-optimized inverse fuzzy model control of OWC wave power plants," *Renewable Energy*, vol. 204, no. 8, pp. 556–568, 2023.

[18] E. Medina-Lopez, A. G. L. Borthwick, A. Moñino, "Analytical and numerical simulations of an oscillating water column with humidity in the air chamber," *Journal of Cleaner Production*, vol. 238, 2019.

[19] J. K. Cochran, H. J. Bokuniewicz, P. L. Yager. Encyclopedia of Ocean Sciences. 3rd Eds. New York: Academic Press, 2019.

[20] M. R. Mia, M. Zhao, H. Wu, H. Palmer, "Numerical simulation of a stationary offshore multi-chamber OWC wave energy converter," *Ocean Engineering*, vol. 265, no. 5, p. 112546, 2022.

[21] G. Cannata, M. Simone, F. Gallerano, "Numerical investigation into the performance of an OWC device under regular and irregular waves," *Journal of Marine Science and Engineering*, vol. 11, no. 4, p. 735, 2023.

[22] D. Satrio, I. K. Aria Pria Utama, Mukhtasor, "The influence of time step setting on the CFD simulation result of vertical axis tidal current turbine," *Journal of Mechanical Engineering and Sciences*, vol. 12, no. 1, pp. 3399–3409, 2018.

[23] J. Aguilar, L. Velásquez, F. Romero, J. Betancour, A. Rubio-Clemente, E. Chica, "Numerical and experimental study of hydrofoil-flap arrangements for hydrokinetic turbine applications," *Journal of King Saud University - Engineering Sciences*, vol. 35, no. 8, pp. 577–588, 2021.

[24] A. I. Montilla-López, L. I. Velásquez-García, J. Betancour, A. Rubio-Clemente, E. L. Chica-Arrieta, "Performance of an Archimedes screw turbine with spiral configuration for hydrokinetic applications," *Revista Facultad de Ingeniería Universidad de Antioquia*, 2022.

[25] A. Posada, E. Chica, L. Vel, L. Velásquez, A. Posada, E. Chica, "Optimization of the basin and inlet channel of a gravitational water vortex hydraulic turbine using the response surface methodology," *Renewable Energy*, vol. 187, pp. 508–521, 2022.

[26] M. Peymani, A. H. Nikseresht, H. B. Bingham, "A 3D numerical investigation of the influence of the geometrical parameters of an I-beam attenuator OWC on its performance at the resonance period," *Energy*, vol. 286, no. 5, p. 129542, 2024.

[27] D. -Z Ning, D. Mu, R. -Q Wang, R. Mayon, "Experimental and numerical investigations on the solitary wave actions on a land-fixed OWC wave energy converter," *Energy*, vol. 282, p. 128363, 2023.

[28] T. S. Phillips, C. J. Roy, "Richardson extrapolation-based discretization uncertainty estimation for computational fluid dynamics," *Journal of Fluids Engineering, Transactions of the ASME*, vol. 136, no. 12, pp. 1-17, 2014.

[29] L. F. Richardson, A. J. Gaunt, "The deferred approach to the limit," *Philosophical Transactions of the Royal Society of London Series A*, vol. 226, no. 6, pp. 299–361, 1927.

[30] C. H. Marchi, M. A. Martins, L. A. Novak, L. K. Araki, M. A. V. Pinto, S. de F. T. Gonçalves, et al., "Polynomial interpolation with repeated Richardson extrapolation to reduce discretization error in CFD," *Applied Mathematical Modelling*, vol. 40, no. 1, pp. 8872–8885, 2016.

[31] S. Vengatesan, P. V. Jeyakarthikeyan, T. Quoc, "Geometrically nonlinear analysis of 2D and 3D structures by a robust Richardson extrapolation based quadrature," *Structures*, vol. 60, no. 9, p. 105951, 2024.

[32] L. P. Da Silva, C. H. Marchi, M. Meneguette, A. C. Foltran, "Robust RRE technique for increasing the order of accuracy of SPH numerical solutions," *Mathematics and Computers in Simulation*, vol. 199, pp. 231–252, 2022.

[33] A. T. Haghighi, A. H. Nikseresht, M. Hayati, "Numerical analysis of hydrodynamic performance of a dual-chamber Oscillating Water Column," *Energy*, vol. 221, p. 119892, 2021.

[34] M. Letzow, Lorenzini, "Numerical analysis of the influence of geometry on a large scale onshore oscillating water column device with associated seabed ramp," *International Journal of Design and Nature and Ecodynamics*, vol. 15, no. 6, pp. 873–884, 2020.

[35] C. Wang, Y. Zhang, "Hydrodynamic performance of an offshore oscillating water column device mounted over an immersed horizontal plate: A numerical study," *Energy*, vol. 222, pp. 1–15, 2021.

[36] M. Hayati, A. H. Nikseresht, A. T. Haghighi, "Sequential optimization of the geometrical parameters of an OWC device based on the specific wave characteristics," *Renewable Energy*, vol. 161, pp. 386–394, 2020.

[37] M. Shahabi-Nejad, A. H. Nikseresht, "A comprehensive investigation of a hybrid wave energy converter including oscillating water column and horizontal floating cylinder," *Energy*, vol. 243, pp. 1–20, 2022.

[38] L. Fu, R. Wang, D. Ning, R. Mayon, "Numerical investigation on the hydrodynamic performance of a land-based OWC system with multi-chamber modules," *Applied Ocean Research*, vol. 141, no. 6, p. 103801, 2023.

[39] X. Zhao, F. Li, J. Zhou, J. Geng, Q. Zou, D. Qin, "Theoretical investigation of hydrodynamic performance of multi-resonant OWC breakwater array," *Applied Ocean Research*, vol. 141, no. 9, pp. 1–19, 2023.

[40] A. A. Medina Rodríguez, R. Silva Casarín, J. M. Blanco Ilzarbe, "The influence of oblique waves on the hydrodynamic efficiency of an onshore OWC wave energy converter," *Renewable Energy*, vol. 183, pp. 687–707, 2022.

[41] J. Zhou, X. Zhao, J. Zang, J. Geng, S. Sun, "Wave power extraction by an oscillating water column array embedded in comb-type breakwaters: Performance analysis and hydrodynamic mechanism," *Physics of Fluids*, vol. 35, no. 7, p. 077110, 2023.

[42] M. M. Samak, H. Elgamal, A. M. N. Elmekawy, "The contribution of L-shaped front wall in the improvement of the oscillating water column wave energy converter performance," *Energy*, vol. 226, p. 120421, 2021.

[43] F. Opoku, M. N. Uddin, M. Atkinson, "A review of computational methods for studying oscillating water columns – the Navier-Stokes based equation approach," *Renewable and Sustainable Energy Reviews*, vol. 174, no. 12, p. 113124, 2023.

[44] M. Kharati-Koopaee, A. Fathi-Kelestani, "Assessment of oscillating water column performance: influence of wave steepness at various chamber lengths and bottom slopes," *Renewable Energy*, vol. 147, pp. 1595–1608, 2020.

[45] H. Palmer, M. Zhao, H. Wu, P. Hu, M. R. Mia, C. Lei, "Improved performance of land-fixed oscillating water column through dual chamber design," *Ocean Engineering*, vol. 290, no. 6, p. 116389, 2023.

[46] L. A. Gallo, E. L. Chica, E. G. Flórez, "Numerical optimization of the blade profile of a savonius type rotor using the response surface methodology," *Sustainability (Switzerland)*, vol. 14, no. 9, pp. 1–18, 2022.

[47] T. Yu, S. He, H. Shi, X. Chen, Q. Guo, "Numerical investigation of hydrodynamic performance and efficiency of a dual-chamber oscillating water column under different damping and chamber breadth ratio combination," *Ocean Engineering*, vol. 266, no. 3, p. 113008, 2022.

[48] A. H. S. Weerakoon, B. H. Kim, Y. J. Cho, D. D. Prasad, M. R. Ahmed, Y. H. Lee, "Design optimization of a novel vertical augmentation channel housing a cross-flow turbine and performance evaluation as a wave energy converter," *Renewable Energy*, vol. 180, pp. 1300–1314, 2021.

[49] B. Bouali, S. Larbi, "Sequential optimization and performance prediction of an oscillating water column wave energy converter," *Ocean Engineering*, vol. 131, no. 1, pp. 162–173, 2017.

[50] Z. Huang, S. Huang, "Two-phase flow simulations of fixed 3D oscillating water columns using OpenFOAM : A comparison of two methods for modeling quadratic power takeoff," *Ocean Engineering*, vol. 232, no. 5, p. 108600, 2021.

[51] Y. Liu, N. Mizutani, Y. H. Cho, T. Nakamura, "Nonlinear hydrodynamic analysis and optimization of oscillating wave surge converters under irregular waves," *Ocean Engineering*, vol. 250, no. 3, p. 110888, 2022.

[52] L. Carlo, C. Iuppa, C. Faraci, "A numerical-experimental study on the hydrodynamic performance of a U-OWC wave energy converter," *Renewable Energy*, vol. 203, pp. 89–101, 2023.

[53] N. Quartier, A. J. C. Crespo, J. M. Domínguez, V. Stratigaki, P. Troch, "Efficient response of an onshore Oscillating Water Column Wave Energy Converter using a one-phase SPH model coupled with a multiphysics library," *Applied Ocean Research*, vol. 115, no. 5, p. 102856, 2021.

[54] X. Chen, J. Cui, M. Y. Li, "Numerical simulation and energy extraction power fitting of OWSCs under regular waves using SPH method," *Ocean Engineering*, vol. 283, no. 6, p. 115077, 2023.

[55] S. C. Bhatia. Advanced Renewable Energy Systems. 1st Ed. New York: WPI Publishing, 2014.

[56] G. F. Weiner, P. R. Teixeira, D. Eric, "Numerical evaluation of optimal sizes of wells turbine and chamber of a cluster of oscillating water columns integrated into a breakwater on the southern Brazilian coast," *Journal of Waterway, Port, Coastal, and Ocean Engineering*, vol. 148, no. 4, p. 4022009, 2022.

[57] K. Trivedi, A. R. Ray, P. A. Krishnan, S. Koley, T. Sahoo, "Hydrodynamics of an OWC device in irregular incident waves using RANS model," *Fluids*, vol. 8, no. 1, pp. 1–31, 2023.

[58] H. Yang, H.-C. Jung, W. Koo, "Oscillating water column (OWC) wave energy converter part 1: Fixed OWC," *Journal of Ocean Engineering and Technology*, vol. 36, no. 4, pp. 280–294, 2022.

[59] A. George, K. Thandayutham, A. Samad, "Numerical analysis of damping induced by impulse turbines for wave energy conversion," *Proceedings of the Institution of Mechanical Engineers, Part M: Journal of Engineering for the Maritime Environment*, vol. 235, no. 2, pp. 448–462, 2021.

[60] U. Izquierdo, G. A. Esteban, J. M. Blanco, I. Albaina, A. Peña, "Experimental validation of a CFD model using a narrow wave flume," *Applied Ocean Research*, vol. 86, no. 12, pp. 1–12, 2019.

[61] U. Izquierdo, L. Galera-Calero, I. Albaina, A. Vázquez, G. A. Esteban, J. M. Blanco, "Experimental and numerical determination of the optimum configuration of a parabolic wave extinction system for flumes," *Ocean Engineering*, vol. 238, no. 5, pp. 1–11, 2021.

[62] D. Kisacik, V. Stratigaki, M. Wu, L. Cappietti, I. Simonetti, P. Troch, et al., "Efficiency and survivability of a floating oscillating water column wave energy converter moored to the seabed: An overview of the EsflOWC MaRINET2 Database," *Water*, vol. 12, no. 4, p. 992, 2020.

[63] R. Mayon, D. Ning, Y. Sun, Z. Ding, R. Wang, Y. Zhou, "Experimental investigation on a novel and hyper-efficient oscillating water column wave energy converter coupled with a parabolic breakwater," *Coastal Engineering*, vol. 185, no. 7, p. 104360, 2023.

[64] A. Rubio, L. Velásquez, E. Chica, "Design of a water channel to model the wave conditions in the Colombian Pacific Ocean," *Renewable Energies & Power Quality Journal*, vol. 20, no. 4, pp. 405–412, 2022.

[65] J. Fredsøe, R. Deigaard. Mechanics of Coastal Sediment Transport. Volume 3. Singapore: World Scientific, 1992.

[66] C. Xu, Z. Liu, G. Tang, "Experimental study of the hydrodynamic performance of a U-oscillating water column wave energy converter," *Ocean Engineering*, vol. 265, no. 8, p. 112598, 2022.

[67] I. Simonetti, L. Cappietti, H. Elsafti, H. Oumeraci, "Optimization of the geometry and the turbine induced damping for fixed detached and asymmetric OWC devices: A numerical study," *Energy*, vol. 139, pp. 1197–1209, 2017.

[68] Z. Deng, C. Wang, P. Wang, P. Higuera, R. Wang, "Hydrodynamic performance of an offshore-stationary OWC device with a horizontal bottom plate: Experimental and numerical study," *Energy*, vol. 187, p. 115941, 2019.

[69] A. Elhanafi, G. Macfarlane, A. Fleming, Z. Leong, "Scaling and air compressibility effects on a three-dimensional offshore stationary OWC wave energy converter," *Applied Energy*, vol. 189, pp. 1–20, 2017.

[70] J. Ding, S. Pang, Z. Chen, "Optimization of the chamber of OWC to improve hydrodynamic performance," *Ocean Engineering*, vol. 287, no. 1–11, p. 115782, 2023.

[71] Y. Theodoro, B. De Lima, N. Gomes, Y. T. B. de Lima, M. D. N. Gomes, L. A. Isoldi, et al., "Geometric analysis through the constructal design of a sea wave energy converter with several coupled hydropneumatic chambers considering the oscillating water column operating principle," *Applied Sciences*, vol. 11, no. 18, p. 8630, 2021.

[72] P. J. Roache. Verification and Validation in Computational Science and Engineering. 1st Ed. United States: Hermosa Publishers, 1998.

[73] A. Meana-Fernández, J. M. Fernández Oro, K. M. Argüelles Díaz, M. Galdo-Vega, S. Velarde-Suárez, "Application of Richardson extrapolation method to the CFD simulation of vertical-axis wind turbines and analysis of the flow field," *Engineering Applications of Computational Fluid Mechanics*, vol. 13, no. 1, pp. 359–376, 2019.

[74] NASA, "Examining spatial convergence (grid)," National Aeronautics and Space Administration, United States, 2021 [Online] Available: https://www.grc.nasa.gov/www/wind/valid/tutorial/spatconv.html

[75] L. Velásquez, A. Posada, E. Chica, "Surrogate modeling method for multi-objective optimization of the inlet channel and the basin of a gravitational water vortex hydraulic turbine," *Applied Energy*, vol. 330, no. 1, p. 120357, 2023.

[76] W. L. Oberkampf, C. J. Roy. Verification and Validation in Scientific Computing. 1st Ed. United Kingdom: Cambridge University Press, 2010.

[77] A. Elhanafi, G. Macfarlane, A. Fleming, Z. Leong, "Experimental and numerical investigations on the hydrodynamic performance of a floating–moored oscillating water column wave energy converter," *Applied Energy*, vol. 205, no. 7, pp. 369–390, 2017.

[78] D. Ning, B. Guo, R. Wang, T. Vyzikas, D. Greaves, D. Zhi Ning, et al., "Geometrical investigation of a U-shaped oscillating water column wave energy device," *Applied Ocean Research*, vol. 97, no. 1, p. 102105, 2020.

[79] S. Tschisgale, T. Kempe, J. Fröhlich, "A general implicit direct forcing immersed boundary method for rigid particles," *Computers and Fluids*, vol. 170, pp. 285–298, 2018.